Engineering 53 (2025) 130–138

Contents lists available at ScienceDirect

Engineering

journal homepage: www.elsevier.com/locate/eng

Research
Artificial Intelligence—Article

A Deep Learning-Based Framework for Environment-Adaptive Navigation of Size-Adaptable Microswarms

Jialin Jiang [a,b], Lidong Yang [c,*], Shihao Yang [a], Li Zhang [a,b,d,e,f,g,*]

[a] Department of Mechanical and Automation Engineering, The Chinese University of Hong Kong, Hong Kong 999077, China
[b] Shenzhen Research Institute, The Chinese University of Hong Kong, Shenzhen 518000, China
[c] Department of Industrial and Systems Engineering, The Hong Kong Polytechnic University (PolyU), Hong Kong 999077, China
[d] Department of Surgery, The Chinese University of Hong Kong, Hong Kong 999077, China
[e] CUHK T Stone Robotics Institute, The Chinese University of Hong Kong, Hong Kong 999077, China
[f] Chow Yuk Ho Technology Center for Innovative Medicine, The Chinese University of Hong Kong, Hong Kong 999077, China
[g] Multi-Scale Medical Robotics Center, Hong Kong Science Park, Hong Kong 999077, China

ARTICLE INFO

Article history:
Received 30 January 2024
Revised 23 September 2024
Accepted 4 November 2024
Available online 2 December 2024

Keywords:
Microswarms
Automatic navigation
Deep learning (DL)

ABSTRACT

Actively controllable microswarms have been a rapidly developing research field with appealing characteristics. Autonomous collision-free navigation of microswarms in confined environments is suitable for various applications, including targeted therapy and delivery. However, several challenges remain unaddressed. First, microswarms possess varying dimensions, and a path planning method suitable to swarms with different dimensions is essential to avoid obstacles. Second, studies on the environment-adaptive navigation of reconfigurable microswarms are limited. Therefore, the planning of the pattern distribution of microswarms based on the local working environment should be examined. This study proposes a deep learning (DL)-based environment-adaptive navigation scheme for swarms. The controller provides reference moving directions for swarms of different sizes in static and dynamic scenarios. Moreover, a pattern-distribution planner was designed to navigate transformable swarms in unstructured environments. To validate the proposed scheme, we applied Fe_3O_4 nanoparticles swarms as a case study. The proposed scheme enables motion and pattern planning for microrobots of multiple sizes and reconfigurability in various working environments, which could foster a general navigation system for reconfigurable microswarms of different sizes.

1. Introduction

Micro/nanorobots can be remotely actuated using external power sources and have attracted increasing research interest because of their promising prospects in biomedicine [1–3]. Benefiting from their miniature size, microrobots can move in narrow and tortuous environments to perform tasks such as minimally invasive surgery [4], targeted delivery [5,6], targeted therapy [7–9], and biosensing [10,11]. Numerous studies have reported targeted delivery using drug-loaded biohybrid microrobots [12] and surface walkers with multiple motion modes in physiologic environments [13]. Moreover, scholars have proposed driving microrobots using chemical fuels [14], acoustic fields [15,16], electric fields [17,18], light [19–21], and magnetic fields [22–24]. Targeted and collision-free navigation of microrobots in confined environments is essential for practical applications. The integration of a path-planning strategy with a motion controller has led to significant developments. The path planning methods adopted for microrobot control can be categorized into offline and online approaches. Offline methods include searching-based (A* [25] and rapid-exploring random tree (RRT) [26]) and iteration-based methods (particle swarm optimization [27,28] and genetic algorithms [29]). Offline methods necessitate long planning and are able to provide optimal trajectories in complicated working environments. Online methods are mostly based on potential fields [30,31]. The optimal moving directions of the agent are generated according to the destination and obstacle distribution. Hence, these methods are suitable for dynamic situations since they enable real-time planning.

* Corresponding authors.
E-mail addresses: lidong.yang@polyu.edu.hk (L. Yang), lizhang@cuhk.edu.hk (L. Zhang).

https://doi.org/10.1016/j.eng.2024.11.020

Despite the impressive progress in steering microrobots in obstacle environments, several challenges remain in swarm navigation. For instance, an adaptive safe distance is essential to avoid collisions when considering the swarms of varying sizes. However, most studies have ignored the physical dimensions of the microrobots. Thus, a strategy suitable for tackling path-planning tasks for agents of different sizes is required. However, most studies treat agents as immutable rigid dots, ignoring gestures and morphological changes. For deformable microrobots (soft robots [32], microrobot swarms [33,34], and magnetic fluid droplets [35]), exploiting reconfigurability according to the surrounding working environment is essential to improving the robustness and adaptability of navigation. However, shape planning introduces additional variables into the system, and analytical methods for addressing this problem are limited.

Deep learning (DL) algorithms provide solutions to these challenges. Owing to the enhanced fitting ability of neural networks, DL algorithms can summarize complicated control policies using abundant training data or interactions [36]. Reinforcement learning (RL) algorithms have been adopted to navigate microrobots in the presence of noise and disturbances [37,38]. DL methods have also been employed for kinetic model fitting and gait optimization of microrobots [39,40].

This study proposes a DL-based autonomous navigation scheme for reconfigurable microswarms of different sizes (Fig. 1(a)). Compared to our previous study [41], a deep reinforcement learning (DRL) algorithm was designed in this study for the real-time navigation of microrobots. The proposed model provides reference directions within a shorter period (approximately 0.1 s) and is more efficient for real-time applications when multiple dynamic obstacles exist. The input image of the model represented the local surroundings obtained from a microscope, and the planning method was suitable for robots of various sizes. However, the previous RRT-based method addressed the safe-distance problem by refining the originally planned paths at a constant distance, which could lack robustness. In addition to motion planning, our scheme includes an environment-adaptive pattern-planning module. In this study, we designed a two-hierarchy deep convolutional neural network (DCNN) based on the boundary distribution of the obstacles and swarm positions to provide an optimal pattern reference for each control period.

2. Microswarms

In this study, we applied two types of Fe_3O_4 swarms as case studies to realize navigation and validate our scheme since the swarm size and pattern distribution are controllable. A microswarm is a dynamic equilibrium of multiple agents under a balance between inter-agent forces and external stimuli. The pattern configuration of magnetic nanoparticle swarms can be tuned by changing the parameters of external magnetic fields [41,42]. Fig. S1 in Appendix A shows the experimental setup used in this study.

Under the actuation of different magnetic fields, the Fe_3O_4 particles exhibited corresponding swarm behaviors. A rotating magnetic field produces a vortex-like swarm, as shown in Fig. 1(b). The magnetized particles formed chain-like structures because of the magnetic force. The chains rotated along each center point, and the induced flow attracted the chains to perform coaxial rotation. Finally, the swarm reaches a balance. Fig. 1(c) shows a ribbon-like swarm triggered by an oscillating magnetic field. The mathematical expression of the field ($\vec{B}$) is:

$$\vec{B} = \vec{B_f} + \vec{B_c} = B_f \cos(2\pi f t)\vec{\imath} + B_c \vec{J} \quad (1)$$

The field is the superposition of the static field $\vec{B_c}$ and the alternating field $\vec{B_f}$. f is the frequency of the field, t is the time. $\vec{\imath}$ and $\vec{J}$ are orthogonal unit vectors. B_f and B_c are the amplitudes of the

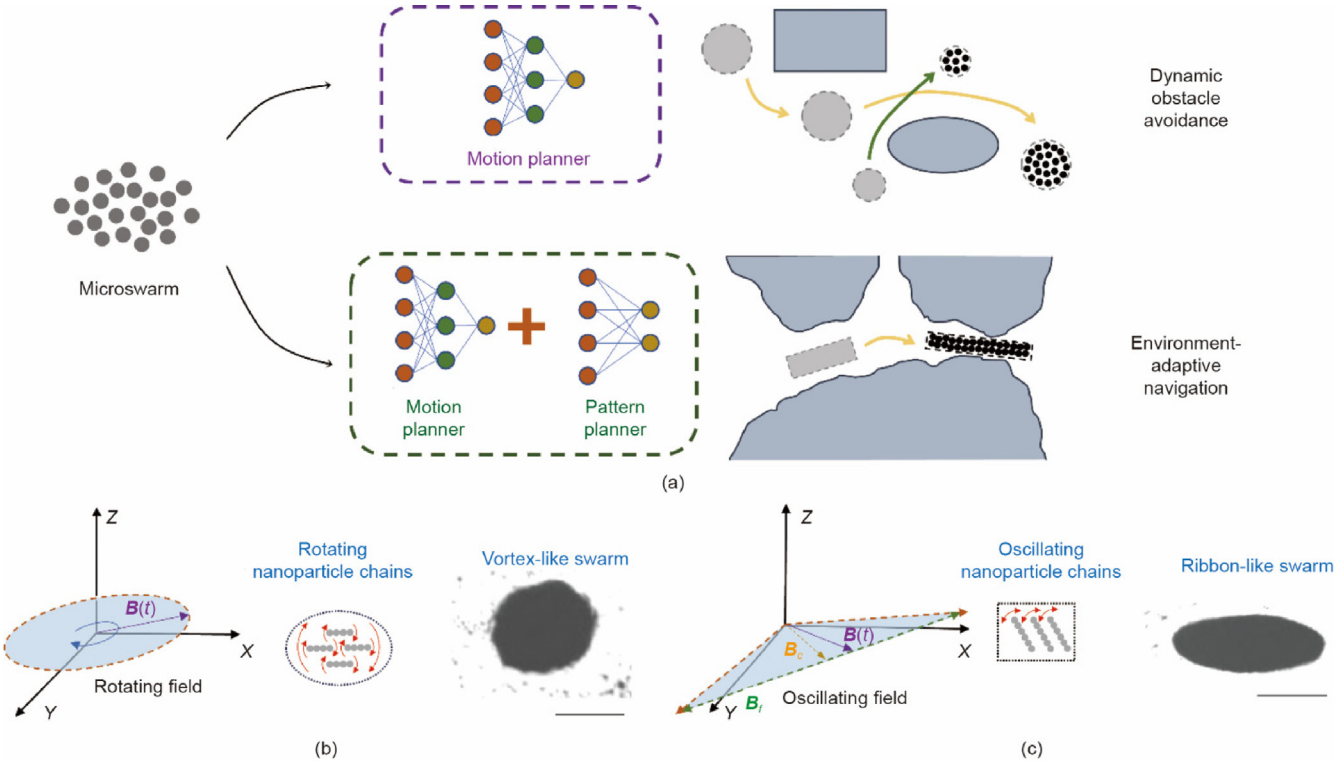

Fig. 1. Demonstration of the swarm navigation. (a) The initial state of the microswarm that involves spreading nanoparticles. The DL-based motion planner and pattern planner govern the obstacle avoidance and environment-adaptive navigation of swarms with different sizes and patterns. (b, c) Two swarm patterns and corresponding actuation fields. Scale bar: 500 μm.

alternating field and the static field, respectively. The chains oscillate along the field, and a swarm is subsequently formed under the chain–chain magnetic force and fluidic interaction.

3. DL-based navigation scheme

3.1. RL-based planning method and control strategy

This study proposes the application of a deep *Q*-network (DQN) scheme for path planning of microrobots. The network provides the optimal moving direction for the robot, given its local surroundings and target position. Compared with conventional planning schemes, RL-assisted methods can conduct online planning tasks and are suitable in channel-like environments and dynamic obstacle scenarios. This method can address planning problems for robots with various dimensions. Note S1 and Fig. S2 in Appendix A present the detailed model and planning method.

To demonstrate that the proposed DQN-based online planning scheme is suitable for microrobots of different sizes, we adopted two agents as case studies: magnetic SiO_2 microbeads and vortex-like microswarms. The diameter of the microbead is 4–5 μm, and that of the swarm is within 300–400 μm. Fig. 2 shows the motion characteristics of the two agents. The SiO_2 microbeads moved in the tumbling mode. The microbead is actuated by a vertical rotating field, the rotation axis is parallel to the *X*–*Y* plane. The vortex-like swarm is triggered by a horizontal rotating field, and the swarm motion is achieved by introducing a pitch angle γ to the field plane, as shown in Fig. 2(b). The velocity and direction of the swarm motion could be modulated by tuning the values of pitch angle γ and yaw angle α. The magnification used for the microbead was 20× and the objective used to monitor the swarm was 2×.

Theoretically, a three-dimensional (3D) Helmholtz coil system can generate precise spatially uniform magnetic fields at the center of the workspace to actuate microrobots. However, the actual field could deviate from the desired value owing to the uncertainty of the coils. Moreover, the installation error of the imaging tools, mechanical vibration, and flow disturbances could yield errors in the direction of the microrobot movement. Thus, we proposed a compensation algorithm to correct the direction of the microrobot movement. Note S2 in Appendix A shows the dynamic model of the microrobots and compensation algorithms. Experiments were conducted to validate the compensation controller, as shown in Fig. S3 in Appendix A.

Table 1 illustrates the model parameters and training conditions. Note S3 in Appendix A presents the training process for the DQN model and Note S4 in Appendix A provides the pseudocode. The model is trained on microrobots of different sizes. Fig. 3 illustrates the resulting success rates. All the training processes were performed separately for our model, and the corresponding network parameters were recorded. During navigation, image-processing methods were adopted, and the areas of the agents were extracted. The adaptivity of the DQN model to agent sizes relies on the loaded parameters. We trained microrobots with four different sizes (1×1, 2×2, 3×3, and 5×5 pixels). The training continues over 30000 episodes, the search success rate for all microrobots exceeded 92%.

A well-trained DQN was utilized for the path planning of microbeads and microswarms. The two agents possessed different dimensions in the field of vision (FOV), indicating that the proposed method can provide an adaptive safe distance for various microrobots and guarantee robust navigation. Python on Spyder IDE was used to program the DQN module. LabVIEW software (National Instruments, USA) was used to develop the main control program. Considering the computational burden of image processing, the control frequency was set to 10 Hz. The real-time requirement could be satisfied because our DQN model requires approximately 0.1 s to complete the planning. For comparison, we present the planning of a conventional rapid random exploring tree method, as shown in Fig. S4 in Appendix A. The computation requires approximately 1.1 s without considering the safe distance, which was unsuitable for the dynamic navigation scenario.

Dynamic obstacle avoidance of microbead: A microbead is placed in the FOV, and the target position is manually given, as shown in Figs. 4(a) and (b). Four virtual obstacles are assigned in the working space, of which two elliptical obstacles and one rectangular obstacle distributed around are static. Two scenarios were considered. In Fig. 4(a), an elliptical obstacle is presented that is designed to move downwards, and in Fig. 4(b), the dynamic part is the irregular cone-shaped region. The trajectories of the microbeads are indicated by red lines. Our proposed planning scheme generated the optimal moving direction online, and the microbeads could effectively avoid obstacles with varying morphological distributions. The microbeads navigated to the target positions. The details can be shown in Video S1 in Appendix A.

Dynamic obstacle avoidance of a microswarm: In this section, a microswarm is utilized as a microrobot agent for a navigation demonstration. Compared to the microbead, the swarm occupies approximately 90×90 pixels in the FOV, indicating that a significant safe distance is crucial to avoid collisions between the swarm boundary and obstacles. Two elliptical obstacles are designed to move toward each other, as depicted in Fig. 4(c). The initial position of the swarm is allocated to the upper right corner of the working space, and the target position is set to the opposite position. The red line indicates the trajectory of the swarm. According to final path, the DQN model tends to navigate the swarm directly to the destination, passing through two obstacles since the interval is relatively large at the beginning. However, as the obstacles move during the navigation, the narrower interval blocks the path, and the algorithm dynamically rearranges the path for the swarm to move rightward and around the obstacle. Finally, the swarm reaches the target region. Fig. S5 in Appendix A illustrates the navigation of a larger swarm. When thrice the number of particles was

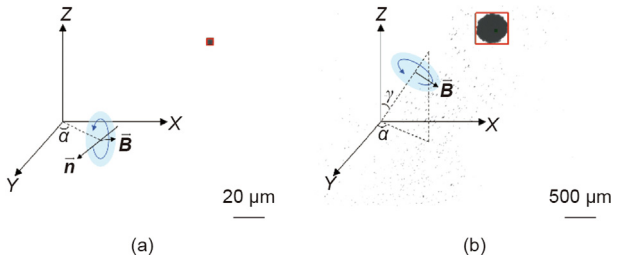

Fig. 2. Motion characteristics of the (a) microbead and (b) microswarm. The microbead locomotes in tumbling mode, and the swarm motion is enabled by the asymmetric friction induced by a pitch angle. $\vec{n}$: normal vector of the magnetic field plane.

Table 1
Parameters of the model and training procedure.

Parameter	Value
Training episodes (N)	30 000
Batch size (B)	128
Memory pool size (N_m)	500 000
Target network parameter update frequency (f_u)	500
Discount factor (γ_l)	0.9
Learning rate (α_l)	1×10^{-4}
Maximum step for one episode	100
Greedy start possibility (ε-greedy algorithm)	0.1
Greedy end possibility (ε-greedy algorithm)	0.9
Greedy decay factor (ε-greedy algorithm)	200

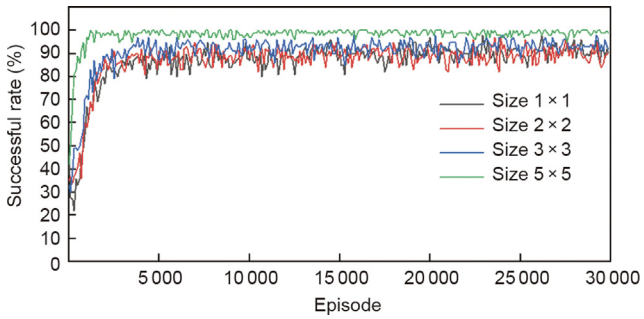

Fig. 3. Searching successful rate of microrobots with four different sizes. The training continues over 30 000 episodes and the final success rates exceed 92%.

used, the diameter of the swarm doubled. The swarm avoids obstacles while approaching the target position. Conventional planning algorithms take the agents as dimensionless dots to provide the trajectories for their central points. In our experiments, the microbeads and swarms were of different sizes and distinct safe distances between the agent's central points and obstacles were required. The results indicated that the proposed DQN model addressed this issue.

Navigate the microswarm in a channel: Experiments were conducted to demonstrate the feasibility of the proposed planning scheme in channel-like environments. A maze-like channel was obtained by laser cutting with a black 3 mm-thick acrylic board. The channel was 18 mm wide and 40 mm long and glued onto a 40 mm × 70 mm silicon wafer. Fig. 4(d) shows the entire structure

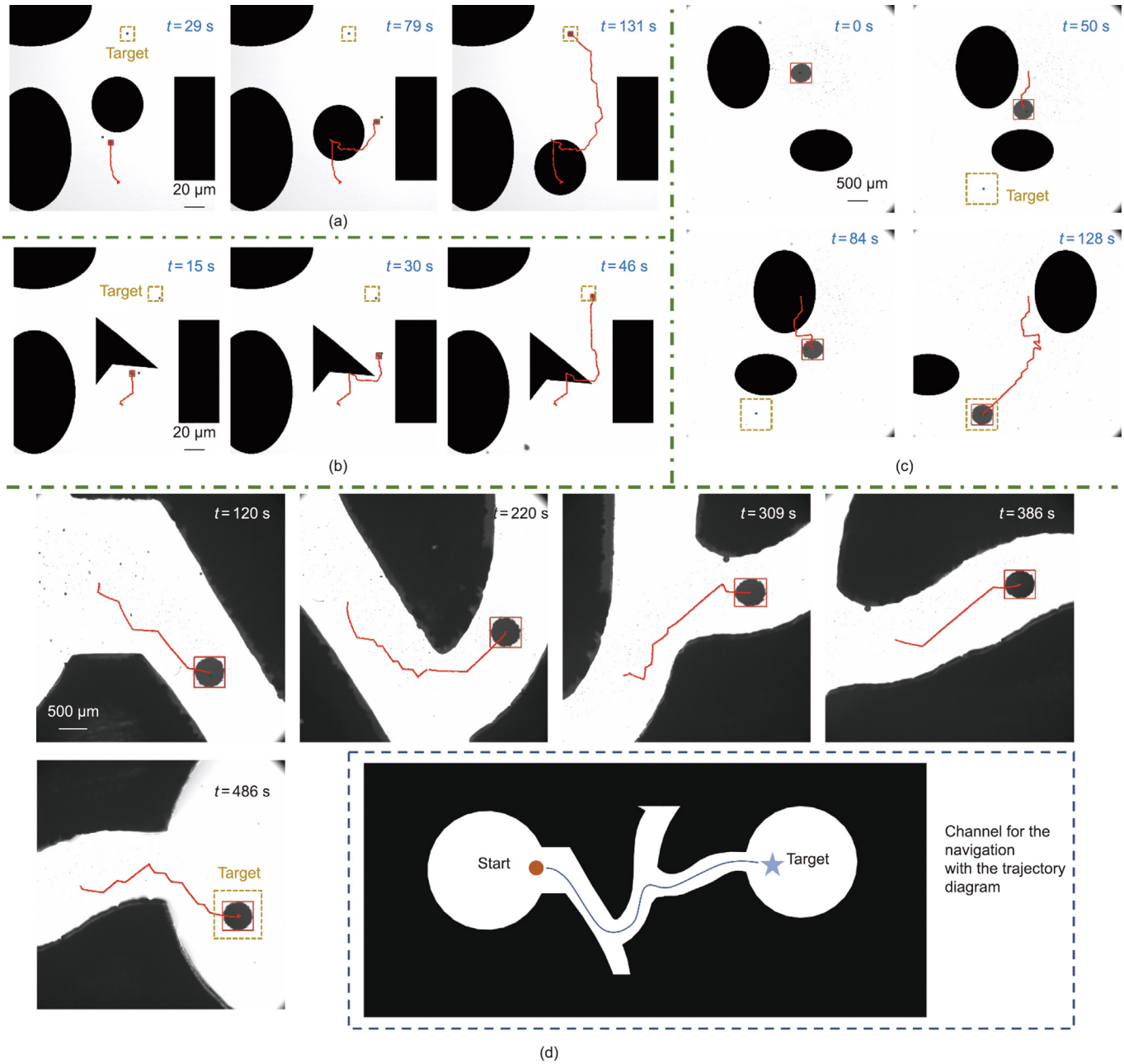

Fig. 4. DQN-based navigation of microrobots. (a, b) The dynamic navigation of a microbead avoiding virtual obstacles with different shapes. (c) The avoidance of two virtual obstacles for a microswarm. (d) Navigate the microswarm in a channel.

of the channel environment. Two round areas were designed as the start and end areas, as illustrated in the figure; the overall trajectory is indicated by a blue line. The FOV of the microscope with a minimum magnification objective lens was 5 mm × 5 mm, which could not effectively cover the entire navigation process. However, a swarm pattern may not exist with an insignificant particle dose. Therefore, the FOV was manually controlled using an *X*–*Y* planar mobile platform, as shown in Fig. S1. The corresponding target position in each local environment is chosen by the operator. Fig. 4(d) illustrates the entire process. According to the red lines showing the trajectories of the swarm, the DQN-based planner can achieve effective navigation with a sufficient safe distance to prevent the swarm from bumping into obstacles.

3.2. DL-assisted swarm pattern planning scheme

In addition to physical dimensions, the environment-adaptive morphology control of transformable microrobot agents was a critical challenge for autonomous navigation. The collision between such non-gradient field-based swarms and obstacles may lead to navigation failure or even the breakdown of the swarms, as depicted in Fig. S6 in Appendix A. Since a microswarm is a dynamic equilibrium consisting of millions of nanoscale agents, its configuration and pattern distribution can be modulated by tuning the actuation field forms and parameters. Reconfigurability grants the swarm enhanced adaptivity to various external working environments. However, exploiting the transformation during navigation to extend the application potential of a microswarm requires more effort. First, obstacle boundary distribution in unstructured environments cannot be described using precise mathematical models. Thus, no analytical solution exists for this optimization problem. Second, quantitative indicators for evaluating the optimality of a swarm pattern that considers nearby obstacles are lacking. This study focused on real-time swarm pattern planning and control by addressing two issues: a cost function to find the optimal swarm distribution at a specific position and a DL-assisted pattern planning scheme. As mentioned in the previous section, a swarm can take two forms. Although the vortex-like swarm exhibits isotropic motion characteristics, the ribbon-like swarm is more stable while changing its morphology during locomotion and its pattern allows superior controllability [43]. Thus, a ribbon-like swarm was adopted as a case study in this section.

An optimal rectangle was utilized to bind the contour points of the swarm boundary. To quantitatively describe the swarm distribution, two variables are proposed: shape ratio γ_{swarm} and orientation angle β_{swarm}. The shape ratio is defined as the ratio of the swarm length to width. The orientation angle β_{swarm} is the angle between the swarm long axis and horizontal direction. The γ_{swarm} of the swarm can be modulated by changing the B_f to B_c ratio. The β_{swarm} coincides with the axis of B_f [44].

Fig. 5 illustrates the navigation of a ribbon-like swarm with pattern planning, highlighting the swarm and next target positions. In our demonstrations, the next target position was determined by fixing the distance (8 pixels in the FOV) along the moving direction obtained from the motion planner. The initial swarm could not pass through the right channel. Therefore, a transformation operation is crucial before the swarm reaches its next target. The main task of the pattern-planning module is to generate an optimal swarm distribution at each waypoint, considering the working environment. We formulated a swarm pattern planning problem as an optimization task. A cost function was presented to define the optimal swarm pattern. A DCNN model was developed to fit the optimal distribution results and generate reference pattern distributions at the given positions (Note S5 and Fig. S7 in Appendix A). The planning scheme is based on the local surroundings of the next given position and the reference ratio of the swarm will taper suddenly when the position is close to obstacles, as illustrated in Fig. S8 in Appendix A. Our DCNN model was trained to generalize across sizes by resizing the feedback images and extracting the local environments, thereby ensuring that the swarm area in the input images was 350 pixels. When the swarm area changed, the range of the extracted local environment changed accordingly, ensuring the adaptability of our DCNN model to various agent sizes. Fig. S9 in Appendix A shows the 100 samples from the virtual environment used to train the DCNN. The method can provide effective planning results in real-time. However, the search method requires several seconds to complete. Fig. S10 in Appendix A illustrates a comparison of consumed time between the traversal searching method and the DCNN-based method.

Additionally, we proposed a DL-based swarm navigation scheme by combining the DQN-based swarm navigation model and the DCNN-assisted swarm pattern planning module. During the motion-control process, the DCNN generated an optimal swarm pattern distribution for each planned waypoint. Fig. 6(a) illustrates an overview of the scheme. First, the working environment was registered to identify obstacles and accessible area information. The DQN model drives the swarm toward the target point. Because the ribbon-like swarm occupies a rectangular area, the DQN model uses a square area with the same side length as the rectangular short edge to represent the swarm position. Since the swarm pattern planning requires a fixed next position and the DQN model only provides the optimal moving direction, distance σ is applied along the planned direction to determine the next waypoint for the swarm pattern planning. An adaptive controller was employed to control the swarm pattern and track the reference distribution. This controller was introduced in a previous study [45]. The experimental setup, planning procedures of the DQN and DCNN models, and the fabrication method of the particles are introduced in Note S6 in Appendix A.

Navigation of a ribbon-like swarm in a free environment: A microswarm was navigated in a free working space, as shown in Fig. 6(b). Two navigation processes were performed, and the corresponding trajectories were marked with pink and purple lines. The red rectangles represent the optimal fittings of the swarm boundary, and the green rectangles represent the planned swarm distributions provided by the DCNN module. As no obstacles existed in the environment, the planned shape ratio remained minimal to

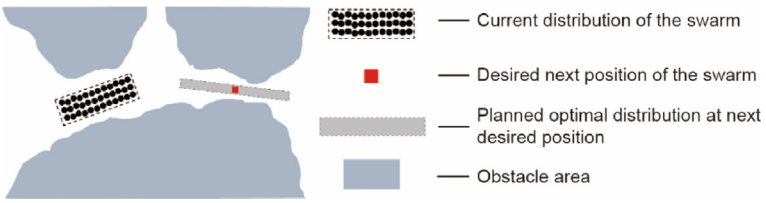

Fig. 5. Navigation process of a ribbon-like swarm considering changing morphology. The position of the next waypoint is given, and the pattern planning module presents the reference swarm distribution according to the local surrounding environments.

yield better swarm stability and a more compact structure. In the meanwhile, the DCNN instructs the swarm to move to the next planned position to avoid unnecessary rotations. Fig. 6(c) shows the real-time swarm-shape ratios of the two navigation processes. The adaptive controller precisely controls the swarm-shape ratio to track the reference value. The output magnetic field ratios are also shown. The field parameters were adaptively tuned to generate stable swarm shape ratio control performance.

Demonstration of the DL-based planning result: The swarm is navigated to bypass the virtual obstacle, as shown in Fig. 7. The blue spot represents the planned waypoint provided by the DQN model. The agent size was fixed at 1 pixel × 1 pixel to ensure that the planned position was close to the obstacle, thereby demonstrating the robustness of our swarm pattern planning method. To prevent the swarm from colliding with an obstacle, the DCNN generates a swarm pattern with the highest shape ratio, as indicated by the green rectangle. An elongated swarm can avoid overlapping and guarantee effective navigation.

Avoidance of dynamic obstacles: Three dynamic virtual obstacles were assigned to the working space. The top two round obstacles moved to the right and upper right, respectively, and the elliptical obstacle below performed a round-trip sinusoidal motion. The target position was provided manually, as illustrated in Fig. 8(a). The DL-based navigation scheme governs the motion control and the optimal gesture and pattern at each waypoint. The DQN model enables real-time motion control in dynamic scenarios,

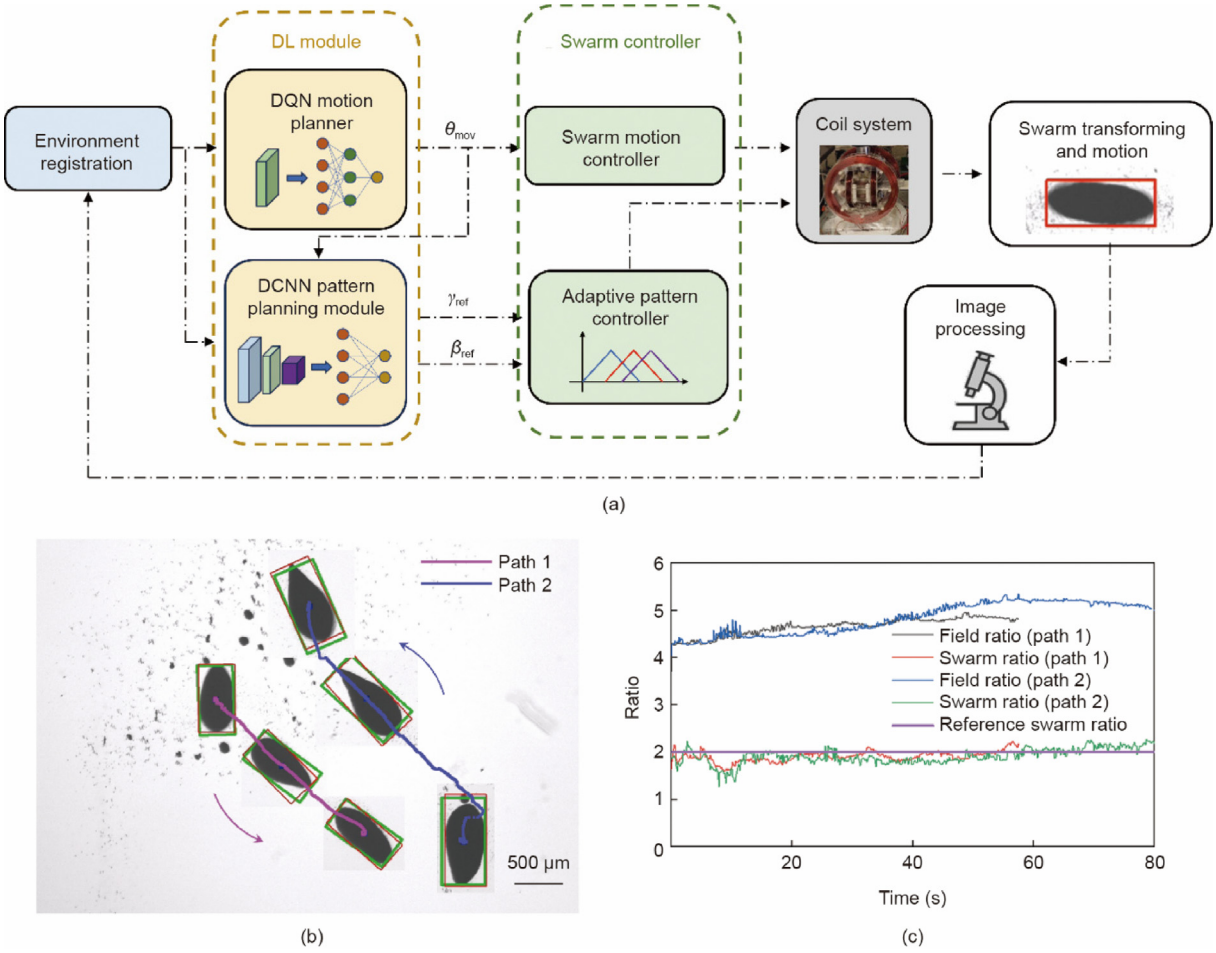

Fig. 6. DL-based navigation framework. (a) The overall diagram of the DL-based autonomous swarm navigation workflow. (b) The DL-based autonomous navigation results of microswarms in a free environment. (c) Under the control of the adaptive controller, the swarm-shape ratio can track the reference value the entire process. θ_{mov}: the reference moving direction; γ_{ref}: the reference shape ratio of the swarm; β_{ref}: the reference orientation angle of the swarm.

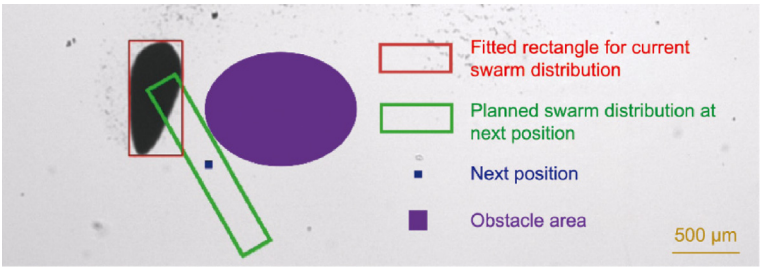

Fig. 7. DL-based swarm navigation results. The motion planning is accomplished by the DQN module, and the swarm pattern planning is achieved by the DCNN. The blue spot represents the planned next position. The DCNN generates a swarm distribution with a shape ratio of 6 because the planned waypoint is close to the virtual obstacle. Elongation allows the swarm to avoid the collision with the obstacle.

and the DCNN plans the swarm pattern according to surrounding obstacles to improve swarm adaptivity. As shown in the trajectory in Fig. 8(a), initially, the distance between the obstacles is not sufficient for the swarm to pass by. After the top two obstacles move away, the swarm is navigated to pass the elliptical obstacle and reach the target.

Navigating the swarm in a channel-like environment: The swarm was controlled to pass through a channel-like environment. The generated reference directions were discretized into eight values; thus, the default pointing angles of the swarm were normally non-optimal or even illegal. Moreover, pattern correction was crucial, particularly in channel scenarios. Fig. 8(b) illustrates the navigation process, comparing the optimal swarm pattern obtained from the DCNN with the original default pattern. The default patterns contain boundary points too close to the channel wall, which may lead to collisions. However, the DCNN modulates the pointing angles of the patterns, guarantees safe distances, and minimizes the rotations between the two swarm states.

Navigating the ribbon-like swarm to pass through a thin channel: The ribbon-like swarm was navigated to pass through a thin channel to demonstrate the swarm shape ratio planning results and the performance of the adaptive swarm pattern controller. Fig. 8(c) illustrates the overall navigation process. The swarm moves from the right side to the left side, and the middle region is a narrow channel in which the swarm tends to elongate itself to obtain a larger shape ratio, thereby allowing a safe distance between the swarm border and channel walls. Fig. 8(d) shows the real-time swarm shape ratios. In the middle region with a green background, the shape ratio was within 3–4. In the open areas on the left and right sides, the swarm shape ratio was

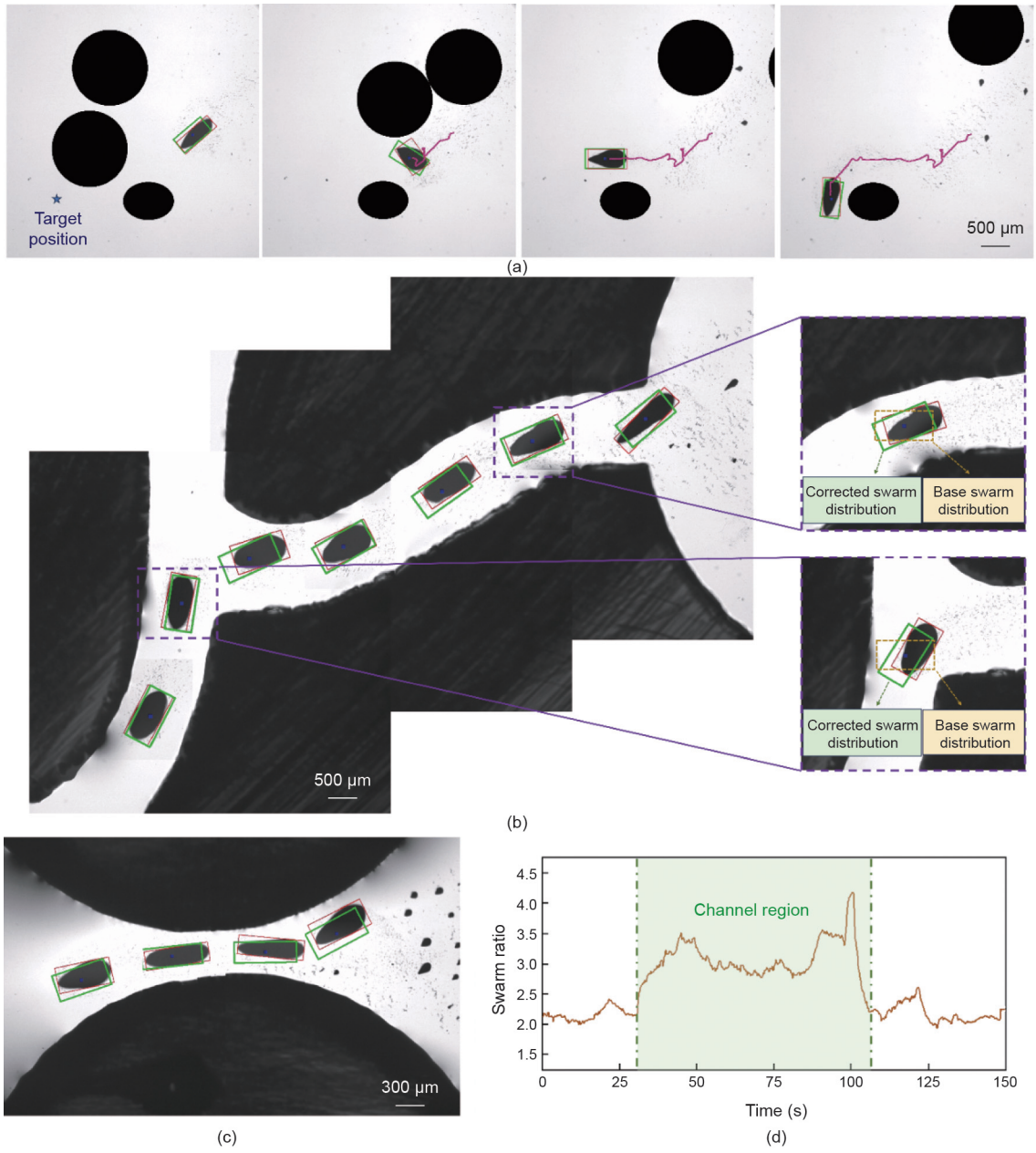

Fig. 8. DL-based navigation. (a) The navigation of a ribbon-like swarm in a dynamic obstacle environment. (b) The autonomous navigation of a ribbon-like swarm in a channel-like environment. (c) Navigation of a ribbon-like swarm passing through a thin channel environment. (d) The real-time swarm shape ratio during the navigation process. The light green region indicates the swarm is at the channel region, and the swarm elongates accordingly.

approximately 2. Therefore, the proposed scheme can provide optimal swarm shape ratio control performance according to the surrounding environment.

4. Conclusions

This study proposed a DL-based autonomous navigation scheme for transformable microrobot agents of different sizes. A RL–DQN model was employed to achieve motion control. Optimal discrete moving directions were generated at each control period by considering the surrounding distribution of the swarm as the input. Additionally, our DQN model can realize effective online motion planning in dynamic scenarios and channel environments, which makes it superior to conventional planning methods. The proposed method was robust against microrobot agents of various sizes. A magnetic SiO_2 microbead and vortex-like microswarm were utilized for case studies to validate the planning method. We propose a swarm pattern planning scheme to further exploit the reconfigurability of microrobots. Considering the transformation ability of the dynamic microrobot swarm, the optimal swarm shape ratio and pointing angle were generated by the proposed DCNN module. By combining these two models, we present a DL-based microrobot navigation scheme. Instead of vortex-like swarms, ribbon-like swarms were applied considering their patterns and distributions. The study results revealed that the swarm elongates to avoid collisions. Moreover, pointing angle correction can guarantee an optimal pattern distribution with a significant safe distance to improve navigation robustness. By combining these two swarm forms, our scheme can navigate the swarm to adapt to various scenarios (vortex-like form for isotropic exploration and ribbon-like form to pass through narrow environments), as illustrated in Fig. S11 in Appendix A. In the future, we will explore the autonomy of microswarms in more practical working environments, including physiologic environments, or in the presence of hydrodynamic disturbances caused by real dynamic obstacles. The optimal moving direction may be attributable to the change in the pattern of the deformable agents. Thus, we will focus on a unified DL model to simultaneously process the locomotion and deformation costs and generate both orders.

CRediT authorship contribution statement

Jialin Jiang: Writing – review & editing, Software. **Lidong Yang:** Writing – review & editing. **Shihao Yang:** Writing – review & editing. **Li Zhang:** Supervision.

Declaration of competing interest

The authors declare that they have no known competing financial interests or personal relationships that could have appeared to influence the work reported in this paper.

Acknowledgment

This work has received funding support from the National Key R&D Program of China (2023YFB4705600), the Hong Kong Research Grants Council (RGC) with Research Impact Fund (R4015-21), the Research Fellow Scheme (RFS2122-4S03), the Strategic Topics Grant (STG1/E-401/23-N, GRF14300621, GRF14301122, GRF14205823, GRF15206223, and GRF25200424), the Guangdong Basic and Applied Basic Research Foundation Project (2023A1515110709), the Research Institute for Advanced Manufacturing (RIAM) of the Hong Kong Polytechnic University (1-CD9F and 1-CDK3), the Startup Fund Project (1-BE9L) of the Hong Kong Polytechnic University, and the MultiScale Medical Robotics Center (MRC) InnoHK, at the Hong Kong Science Park, the SIAT-CUHK Joint Laboratory of Robotics and Intelligent Systems.

Appendix A. Supplementary data

Supplementary data to this article can be found online at https://doi.org/10.1016/j.eng.2024.11.020.

References

[1] Nelson BJ, Kaliakatsos IK, Abbott JJ. Microrobots for minimally invasive medicine. Annu Rev Biomed Eng 2010;12:55–85.
[2] Sitti M, Ceylan H, Hu W, Giltinan J, Turan M, Yim S, et al. Biomedical applications of untethered mobile milli/microrobots. Proc IEEE 2015;103(2):205–24.
[3] Palagi S, Fischer P. Bioinspired microrobots. Nat Rev Mater 2018;3(6):113–24.
[4] Li Z, Feiling J, Ren H, Yu H. A novel tele-operated flexible robot targeted for minimally invasive robotic surgery. Engineering 2015;1(1):73–8.
[5] Khalil ISM, Klingner A, Hamed Y, Hassan YS, Misra S. Controlled noncontact manipulation of nonmagnetic untethered microbeads orbiting two-tailed soft microrobot. IEEE Trans Robot 2020;36(4):1320–32.
[6] Jing W, Chowdhury S, Guix M, Wang J, An Z, Johnson BV, et al. A microforce-sensing mobile microrobot for automated micromanipulation tasks. IEEE Trans Autom Sci Eng 2019;16(2):518–30.
[7] Sun M, Chan KF, Zhang Z, Wang L, Wang Q, Yang S, et al. Magnetic microswarm and fluoroscopy-guided platform for biofilm eradication in biliary stents. Adv Mater 2022;34(34):2201888.
[8] Wang B, Chan KF, Yuan K, Wang Q, Xia X, Yang L, et al. Endoscopy-assisted magnetic navigation of biohybrid soft microrobots with rapid endoluminal delivery and imaging. Sci Robot 2021;6(52):eabd2813.
[9] Wang M, Wu T, Liu R, Zhang Z, Liu J. Selective and independent control of microrobots in a magnetic field: a review. Engineering 2023;24:21–38.
[10] Yang L, Zhang Y, Wang Q, Zhang L. An automated microrobotic platform for rapid detection of *C. diff* toxins. IEEE Trans Biomed Eng 2020;67(5):1517–27.
[11] Zhang Y, Zhang L, Yang L, Vong CI, Chan KF, Wu WKK, et al. Real-time tracking of fluorescent magnetic spore-based microrobots for remote detection of *C. diff* toxins. Sci Adv 2019;5(1):eaau9650.
[12] Li T, Yu S, Sun B, Li Y, Wang X, Pan Y, et al. Bioinspired claw-engaged and biolubricated swimming microrobots creating active retention in blood vessels. Sci Adv 2023;9(18):eadg4501.
[13] Wang H, Liu C, Yang X, Ji F, Song W, Zhang G, et al. Multimode microdimer robot for crossing tissue morphological barrier. iScience 2023;26(11):108320.
[14] Lin X, Xu B, Zhu H, Liu J, Solovev A, Mei Y. Requirement and development of hydrogel micromotors towards biomedical applications. Research 2020;2020:7659749.
[15] Sabrina S, Tasinkevych M, Ahmed S, Brooks AM, de la Cruz MO, Mallouk TE, et al. Shape-directed microspinners powered by ultrasound. ACS Nano 2018;12(3):2939–47.
[16] Ahmed D, Baasch T, Jang B, Pane S, Dual J, Nelson BJ. Artificial swimmers propelled by acoustically activated flagella. Nano Lett 2016;16(8):4968–74.
[17] Liu R, Wong F, Duan W, Sen A. Enhanced electrophoretic motion using supercapacitor-based energy storage system. Adv Mater 2013;25(48):6997–7002.
[18] Freedman KJ, Otto LM, Ivanov AP, Barik A, Oh SH, Edel JB. Nanopore sensing at ultra-low concentrations using single-molecule dielectrophoretic trapping. Nat Commun 2016;7:10217.
[19] Qian B, Montiel D, Bregulla A, Cichos F, Yang H. Harnessing thermal fluctuations for purposeful activities: the manipulation of single micro-swimmers by adaptive photon nudging. Chem Sci 2013;4(4):1420–9.
[20] Zhang S, Scott EY, Singh J, Chen Y, Zhang Y, Elsayed M, et al. The optoelectronic microrobot: a versatile toolbox for micromanipulation. Proc Natl Acad Sci USA 2019;116(30):14823–8.
[21] Zhou D, Zhuang R, Chang X, Li L. Enhanced light-harvesting efficiency and adaptation: a review on visible-light-driven micro/nanomotors. Research 2020;2020:6821595.
[22] Diller E, Giltinan J, Lum GZ, Ye Z, Sitti M. Six-degree-of-freedom magnetic actuation for wireless microrobotics. Int J Robot Res 2016;35(1–3):114–28.
[23] Li J, Li X, Luo T, Wang R, Liu C, Chen S, et al. Development of a magnetic microrobot for carrying and delivering targeted cells. Sci Robot 2018;3(19):eaat8829.
[24] Oulmas A, Andreff N, Régnier S. 3D closed-loop swimming at low reynolds numbers. Int J Robot Res 2018;37(11):1359–75.
[25] Yang Z, Yang L, Zhang L. Autonomous navigation of magnetic microrobots in a large workspace using mobile-coil system. IEEE/ASME Trans Mechatron 2021;26(6):3163–74.
[26] Zheng L, Jia Y, Dong D, Lam W, Li D, Ji H, et al. 3D navigation control of untethered magnetic microrobot in centimeter-scale workspace based on field-of-view tracking scheme. IEEE Trans Robot 2022;38(3):1583–98.
[27] Yang L, Zhang Y, Wang Q, Chan KF, Zhang L. Automated control of magnetic spore-based microrobot using fluorescence imaging for targeted delivery with cellular resolution. IEEE Trans Autom Sci Eng 2020;17(1):490–501.

[28] Wang Q, Yang L, Zhang L. Micromanipulation using reconfigurable self-assembled magnetic droplets with needle guidance. IEEE Trans Autom Sci Eng 2022;19(2):759–71.
[29] Xie H, Fan X, Sun M, Lin Z, He Q, Sun L. Programmable generation and motion control of a snakelike magnetic microrobot swarm. IEEE/ASME Trans Mechatron 2019;24(3):902–12.
[30] Kim H, Cheang UK, Kim MJ. Autonomous dynamic obstacle avoidance for bacteria-powered microrobots (BPMs) with modified vector field histogram. PLoS One 2017;12(10):e0185744.
[31] Lee J, Zhang X, Park CH, Kim MJ. Real-time teleoperation of magnetic force-driven microrobots with 3D haptic force feedback for micro-navigation and micro-transportation. IEEE Robot Autom Lett 2021;6(2):1769–76.
[32] Sun M, Tian C, Mao L, Meng X, Shen X, Hao B, et al. Reconfigurable magnetic slime robot: deformation, adaptability, and multifunction. Adv Funct Mater 2022;32(26):2112508.
[33] Jin D, Zhang L. Collective behaviors of magnetic active matter: recent progress toward reconfigurable, adaptive, and multifunctional swarming micro/nanorobots. Acc Chem Res 2022;55(1):98–109.
[34] Wang L, Gao H, Sun H, Ji Y, Song L, Jia L, et al. Reconfigurable vortex-like paramagnetic nanoparticle swarm with upstream motility and high body-length ratio velocity. Research 2023;6:0088.
[35] Zhang W, Deng Y, Zhao J, Zhang T, Zhang X, Song W, et al. Amoeba-inspired magnetic venom microrobots. Small 2023;19(23):2207360.
[36] Li K, Meng MQH. Personalizing a service robot by learning human habits from behavioral footprints. Engineering 2015;1(1):79–84.
[37] Muiños-Landin S, Fischer A, Holubec V, Cichos F. Reinforcement learning with artificial microswimmers. Sci Robot 2021;6(52):eabd9285.
[38] Colabrese S, Gustavsson K, Celani A, Biferale L. Flow navigation by smart microswimmers via reinforcement learning. Phys Rev Lett 2017;118(15):158004.
[39] Xu T, Liu J, Huang C, Sun T, Wu X. Discrete-time optimal control of miniature helical swimmers in horizontal plane. IEEE Trans Autom Sci Eng 2022;19(3):2267–77.
[40] Demir SO, Culha U, Karacakol AC, Pena-Francesch A, Trimpe S, Sitti M. Task space adaptation via the learning of gait controllers of magnetic soft millirobots. Int J Robot Res 2021;40(12–14):1331–51.
[41] Yu J, Yang L, Zhang L. Pattern generation and motion control of a vortex-like paramagnetic nanoparticle swarm. Int J Robot Res 2018;37(8):912–30.
[42] Yang L, Jiang J, Gao X, Wang Q, Dou Q, Zhang L. Autonomous environment-adaptive microrobot swarm navigation enabled by deep learning-based real-time distribution planning. Nat Mach Intell 2022;4(5):480–93.
[43] Yu J, Wang B, Du X, Wang Q, Zhang L. Ultra-extensible ribbon-like magnetic microswarm. Nat Commun 2018;9(1):3260.
[44] Yang L, Yu J, Zhang L. Statistics-based automated control for a swarm of paramagnetic nanoparticles in 2-D space. IEEE Trans Robot 2020;36(1):254–70.
[45] Yu J, Yang L, Du X, Chen H, Xu T, Zhang L. Adaptive pattern and motion control of magnetic microrobotic swarms. IEEE Trans Robot 2022;38(3):1552–70.